ARTICLES

Femtosecond Pump−Probe Studies of Dichlorine Monoxide in Solution

Catherine C. Cooksey and Philip J. Reid*

Department of Chemistry, University of Washington, Box 351700, Seattle, Washington 98195

Received: February 17, 2003; In Final Form: May 1, 2003

The first femtosecond pump−probe studies of ClOCl photochemistry in solution are presented. Following 266-nm photoexcitation of ClOCl dissolved in perfluorohexane, the resulting evolution in optical density is monitored at seven wavelengths ranging from 266 to 400 nm. A depletion in optical density consistent with ground-state ClOCl photolysis is observed, followed by increases in optical density at 266 and 315 nm assigned to the production of ClO and ClClO, respectively. Kinetic analysis of the temporal evolution in optical density establishes that photoproduct appearance occurs on the ∼10-ps time scale. Later time decay of the optical density at 315 nm is mirrored by a corresponding increase in optical density at 266 nm consistent with thermal decomposition of ClClO to produce ClO and Cl on the ∼100-ps time scale. The quantum yields for photoproduct formation are determined through analysis of the absolute change in optical density. This analysis establishes that the quantum yields for ClClO and ClO production are 0.4 ± 0.1 and 0.6 ± 0.1, respectively. Finally, the observation of ClClO production following ClOCl photoexcitation is similar to the behavior observed for chlorine dioxide (OClO) suggesting that photoisomerization is a general feature of halooxide reactivity in solution.

Introduction

Halooxide photochemistry is of interest due to the participation of these compounds in a variety of atmospheric processes.[1−4] The environmental impact of these compounds results from their ability to photochemically produce atomic halogens, with the extent of halogen production dependent on the environment in which the chemistry occurs. For example, photolysis of chlorine dioxide (OClO) promotes dissociation to form ClO and O, or Cl and O_2.[5,6] In the gas phase, the quantum yield for atomic chlorine production is modest with $\Phi = 0.04$; however, in condensed environments the quantum yield increases to $\Phi = 0.1$ and unity in aqueous solution and ice, respectively. Current interest involves elucidating the fundamental reasons behind this behavior in order to understand the environmental impact of halooxides in both homogeneous and inhomogeneous settings.

Of interest here is the photochemical reaction dynamics of dichlorine monoxide (ClOCl). It is believed that this compound plays only a minor role in stratospheric chemistry. It is the anhydrous form of hypochlorous acid (HOCl), a chlorine reservoir species,[7] and ClOCl is used as a convenient photolytic source of ClO in laboratory studies.[8] The photochemistry of ClOCl provides a comparative example with respect to other halooxides including OClO. Studies of gaseous OClO have demonstrated that photolysis leads predominately to ClO and O.[9−20] However, in low-temperature matrixes, photochemical production of the structural isomer, ClOO, occurs to an appreciable extent.[21−24] Solution photochemistry represents an intermediate case in which both ClO/O and ClOO production occurs, with geminate recombination of the ClO/O photofragments also occurring resulting in re-formation of the parent molecule.[25−35] While geminate recombination and photoisomerization are central to the reactivity of OClO, it is unclear if this behavior is reflected by other halooxides such as ClOCl.

Our knowledge regarding ClOCl photochemistry is limited, with only a few gas phase and in matrix isolation studies presented in the literature.[22,36−47] Nelson et al. studied the gas-phase dissociation of ClOCl using photofragment translational energy spectroscopy with photoexcitation at 308, 248, and 198 nm.[40] Dissociation to form ClO and Cl was observed exclusively with photoexcitation at 308 nm. However, with photoexcitation at 248 nm, an additional channel was observed and assigned to vibrationally excited ClO that undergoes secondary dissociation to form Cl and O(^{3}P). Finally, two distinct photochemical channels were observed following 198-nm photoexcitation involving Cl_2 formation with atomic oxygen produced as either O(^{3}P) or O(^{1}D). Broadband flash photolysis studies of Nickolaisen and co-workers were performed in which the yield of ClO as a function of bath gas pressure was determined.[41] The ClO yield was observed to decrease with increasing pressure for wavelengths greater than 300 nm leading to the suggestion that photoexcitation of ClOCl at wavelengths greater than 300 nm results in rapid intersystem crossing to two triplet states from which dissociation to form ClO and Cl or internal conversion to the ground state occurs. Tanaka et al. have used photofragment ion imaging to investigate the primary photochemistry of gas-phase ClOCl following excitation at 235 nm and found that production of the lowest-velocity Cl atoms was consistent with a three-body fragmentation process.[43] Finally, Molina and co-workers have recently measured the quantum yields of ClO and Cl production using chemical ionization mass

* To whom correspondence should be addressed. E-mail: preid@chem.washington.edu.

10.1021/jp030213l CCC: $25.00
Published on Web 06/26/2003

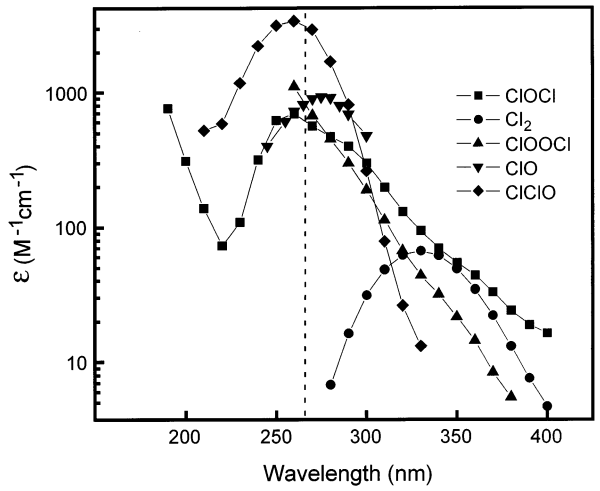

Figure 1. Absorption spectra of ClOCl and its potential photoproducts: Cl_2, ClOOCl, ClO, and ClClO. The molar absorptivity values are those of ClOCl dissolved in carbon tetrachloride.[55] The gas-phase absorption spectra of Cl_2, ClOOCl, and ClO are taken from the literature.[51,54] The absorption spectrum of ClClO is for this species isolated in an argon matrix.[46] The dashed line indicates the excitation wavelength employed in these studies.

spectrometry following photolysis of gaseous ClOCl at 320, 360, 400, and 440 nm.[44] When normalized to the quantum yield for ClO and Cl production at 255 nm, it was found that the ClO production quantum yield demonstrates little actinic-wavelength dependence. In addition, these authors concluded that the photochemical behavior could be interpreted entirely in terms of transitions between singlet states, in opposition to the triplet-state mechanism suggested by Nicolaisen et al.

The first matrix isolation studies of ClOCl were performed by Rochkind and Pimentel.[22] In this work, ClOCl in low-temperature nitrogen and argon matrixes was photolyzed, and the resulting reaction mixture was probed by IR and Raman spectroscopy. It was established that photolysis of ClOCl results in formation of the structural isomer, ClClO, and the ClO dimer. Johnsson et al. reported the first UV absorption spectra of ClClO formed by the photolysis of ClOCl in an argon matrix.[46] Subtraction of the UV spectra before and after photolysis was performed to determine the UV absorption spectrum of ClClO ($\lambda_{max} = 260$ nm). In addition, using the absorption cross section of gaseous ClOCl at 260 nm, an estimate for the ClClO maximum absorption cross section of 1.3×10^{-17} cm^2/molecule was obtained.

There is very little information regarding the reaction dynamics of ClOCl in solution. The first studies of ClOCl in solution were performed in the 1930s,[48] with further studies not performed until recently. In this recent work, Esposito et al.[49] obtained the resonance Raman spectrum of ClOCl in CCl_4. Using 282.4-nm excitation, they investigated the dependence of the resonance Raman spectra on incident pulse energy and observed scattering assignable to both ClClO and ClO. The power dependence of photoproduct formation was investigated and found to be consistent with both ClClO and ClO being primary photoproducts of ClOCl.

In this paper, we present the first femtosecond transient absorption study of ClOCl photochemistry in solution. The evolution in optical density following ClOCl photolysis at 266 nm is monitored at seven probe wavelengths ranging from 266 to 400 nm. The absorption spectra of the parent species and all potential photoproducts observed in studies performed to date are presented in Figure 1. The figure demonstrates that the probe wavelengths employed here provide good coverage of the spectral range over which optical-density evolution associated with photoproduct formation is expected to occur. Following ClOCl photoexcitation, substantial increases in optical density are observed at 315 and 266 nm and are assigned to ClClO and ClO, respectively. Kinetic analysis of this evolution reveals that both photoproducts appear on the ~10 ps time scale. In addition to these dynamics, later-time decomposition of ClClO to produce ClO and Cl is observed on the ~100 ps time scale. Given these results, a photochemical model is presented in which ClOCl dissociates to form ClO and Cl or undergoes photoisomerization to produce ClClO that undergoes subsequent ground-state thermal dissociation to produce ClO and Cl. With this model, quantum yields for ClClO and ClO production of 0.4 ± 0.1 and 0.6 ± 0.1, respectively, are established. Finally, the solution phase photochemistry of ClOCl is compared to that of OClO. The production of ClClO observed here mirrors the production of ClOO following OClO photolysis suggesting that photoisomerization is a general feature of halooxide photochemistry in solution.

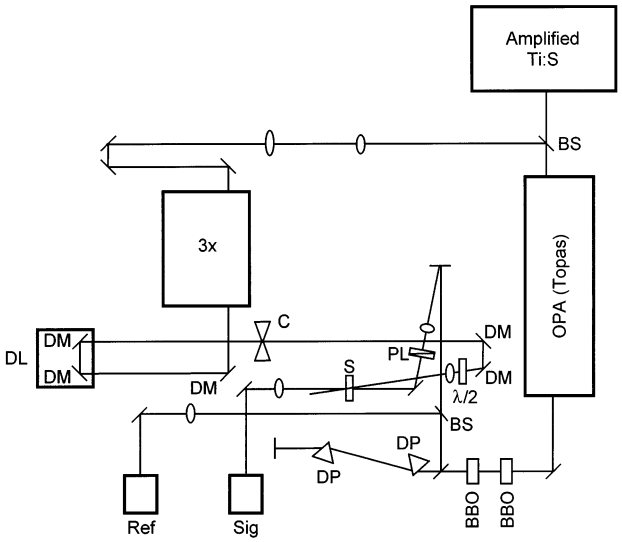

Figure 2. Schematic of the pump−probe spectrometer employed in this work. The following abbreviations have been used: BBO, frequency doubling β-barium borate crystal; BS, beam splitter; C, mechanical chopper; DL, optical delay line; DM, dichroic mirror; DP, Brewster dispersion prisms; $\lambda/2$, zero-order half-wave plate; OPA, optical parametric amplifier; 3×, frequency tripler; PL, calcite polarizer; S, sample.

Experimental Section

A schematic diagram of the pump−probe spectrometer is presented in Figure 2. An intracavity doubled Nd:VO_4 laser (Spectra Physics Millenia V) was used to pump a home-built Ti:sapphire oscillator that produced 30-fs pulses (full width at half-maximum (fwhm)) centered at 780 nm at a repetition rate of 91 MHz. Amplification of these pulses was performed using the chirped-pulse technique (Clark-MXR CPA-1000-PS). The postcompression amplified output consisted of 85-fs fwhm pulses centered at 780 nm with pulse energy of 850 μJ at a repetition rate of 1 kHz.

The amplified output was split into two components. Twenty percent of the output was frequency tripled (Spectra Physics TP-IA) to generate the actinic field. The remainder of the amplified output was used to generate the probe field. For probe wavelengths at 400 and 266 nm, the amplified output was frequency doubled and tripled, respectively. For probe wavelengths from 286 to 350 nm, the fourth harmonic of the signal

TABLE 1: Kinetic Parameters Determined from Analysis of the Pump−Probe Data for ClOCl Dissolved in Perfluorohexane

λ_{pr}[a] (nm)	A_1[b]	t_1 (ps)	A_2	t_2 (ps)	A_3	t_3 (ps)
266	-0.11 ± 0.06[c]	9.6 ± 6.1	-0.35 ± 0.13	122.8 ± 78.6	0.53 ± 0.16	offset[d]
286	-0.40 ± 0.15	8.8 ± 2.9	0.60 ± 0.15	>1000		
300	-0.38 ± 0.12	11.4 ± 4.3	0.33 ± 0.15	41.6 ± 35.5	0.29 ± 0.27	381.6 ± 94.7
317	-0.47 ± 0.06	9.3 ± 4.3	0.42 ± 0.06	26.4 ± 6.2	0.12 ± 0.09	199.3 ± 118.3
350	-0.54 ± 0.07	3.2 ± 3.3	0.33 ± 0.12	28.3 ± 12.6	0.13 ± 0.05	196.2 ± 56.9
400	-0.99 ± 0.0003	0.14 ± 0.10	-0.0001 ± 0.0002	7.9 ± 3.4	0.0002 ± 0.0002	20.1 ± 6.7

[a] Wavelength at which the transient change in optical density was measured. [b] Amplitudes are normalized such that $\sum|A_i| = 1$. [c] Errors represent 1 standard deviation from the mean of all measurements employed at a given wavelength. [d] A time constant of 10 000 ps was included to represent any persistent offset in optical density at long delay times.

field from an optical parametric amplifier (OPA, Quantronix TOPAS) was employed. Isolation of the signal fourth harmonic was accomplished using a pair of CaF_2 prisms that also provided precompensation for group-velocity dispersion of the probe field. Following the prism pair, a beam splitter separated the probe into the sample and reference beams. A calcite polarizer was placed in the probe line to define the polarization. The pump beam was temporally adjusted relative to the probe beam using a delay stage. The pump polarization was oriented to 54.7° relative to the probe using a zero-order half-wave plate to minimize the contribution of rotational dynamics to the data.

Pump and probe pulse energies of 4.5 and 0.2 μJ, respectively, were employed. The optical-density changes were found to vary linearly with pump power. The focus of the pump beam was adjusted so that the probe beam waist was approximately five times smaller than that of the pump at the sample. The instrument response was measured by the optical Kerr effect in water and was 350 ± 50 fs for all probe wavelengths. Samples were delivered to a fused-silica flow cell with CaF_2 windows having a path length of 0.2 mm. The flow rate was sufficient to replenish the sample volume between actinic events.

Measurement of the pump-induced change in sample optical density was performed as follows. The sample and reference probe signals were detected with UV-enhanced photodiodes (Advanced Photonix, Inc. SD 200-13-23-242). The photodiode outputs were processed by gated integration (Stanford Research Systems SR250) and subtracted on a shot to shot basis. A mechanical chopper operating at half the amplifier repetition frequency modulated the pump beam, and the gated-integrator output was delivered to a computer where the voltage difference between adjacent laser shots (i.e., pump on versus pump off) was determined providing a measure of the pump-induced optical-density change. Up to 1000 laser shots per time point were acquired for an individual scan, with three or four scans averaged to produce the data shown here. A convolution of the instrument response with a sum of exponentials was fit to the data using the Levenberg−Marquardt algorithm. Goodness of the fit was judged by χ^2 values as well as visual inspection of the residuals. Errors reported here correspond to one standard deviation of the mean of multiple measurements taken (five or greater).

Samples of dichlorine monoxide (ClOCl) dissolved in perfluorohexane (PFH) were prepared following a modified version of the method outlined by Cady.[50] Chlorine gas (99%, JCI Jones Chemicals) was bubbled into a flask containing 50 mL of PFH (Acros) cooled in a dry ice−acetonitrile bath. Under the assumption that the molar absorptivity of Cl_2 in PFH is the same as in CCl_4, Cl_2 concentrations of 0.75 M were generated as determined by UV−vis absorption. Yellow mercuric oxide (Acros) was then added to the Cl_2 solution at a molar ratio of 1.1 HgO to Cl_2, and this mixture was stirred over an ice bath for at least 45 min. Formation of ClOCl was evidenced by a change in solution color from green to reddish brown. After the reaction, the mercuric oxide was allowed to settle to the bottom of the flask and the solution of ClOCl in PFH was decanted, resulting in 35−40 mL of stock solution. Stock solutions were typically 0.2−0.3 M in ClOCl as determined by UV−vis absorption and would undergo decomposition into mainly chlorine dioxide within 1−2 days. To minimize the decomposition rate, stock solutions were further diluted with PFH until a ClOCl concentration of ~0.05 M was reached. This diluted stock solution would last 1 week in the freezer. Further dilution of these solutions was performed to produce the 7.2 mM solutions used in the pump−probe work. The results reported here were determined to be identical with ~2-fold changes in concentration. The concentration of the sample was monitored at the start and end of the experiment, and the sample was kept at ~0° C during the experiment using an ice bath. In addition to the kinetic studies described above, the absolute change in optical density at each probe wavelength was determined employing a fresh 5.0 mM sample of ClOCl in PFH to minimize variation in sample concentration in this absolute comparative study.

Results

Figure 3 depicts the time evolution in optical density observed following 266-nm photolysis of ClOCl in perfluorohexane. Representative probe wavelengths at 266, 286, 300, 317, 350, and 400 nm are presented in the figure. To simplify presentation, the results are discussed with respect to three wavelength regions, 266−300 nm, 300−350 nm, and greater than 350 nm.

266 nm ≤ λ_{pr} < 300 nm. In this wavelength region, both photoinduced ground-state ClOCl depletion and photoproduct formation are observed. At 266 nm, an initial decrease in optical density is observed consistent with the depletion of ground-state ClOCl due to photolysis. Following this initial decrease, an increase in optical density is observed that persists out to the longest delays investigated (500 ps). The evolution in optical density observed at 266 nm was fit to a sum of three exponentials convolved with the instrument response resulting in appearance time constants of 9.6 ± 6.1 and 122.8 ± 78.6 ps and a long time offset. The time constants determined for this and other probe wavelengths are presented in Table 1. At 286 nm, an increase in optical density is observed that appears with a time constant of 8.8 ± 2.9 ps. Scans out to longest delays suggest that there may be an extremely modest increase in optical density occurring at long times, with a time constant for this evoltion being >1000 ps.

300 nm ≤ λ_{pr} < 350 nm. The evolution in optical density observed in this wavelength region is dominated by photoproduct appearance and decay. At 300 nm, a substantial increase in optical density occurs with a time constant of 11.4 ± 4.3 ps and then undergoes biexponential decay with time constants of 41.6 ± 35.5 and 381.6 ± 94.7 ps. Similar behavior is observed at 317 nm, where the increase in optical density occurs with a

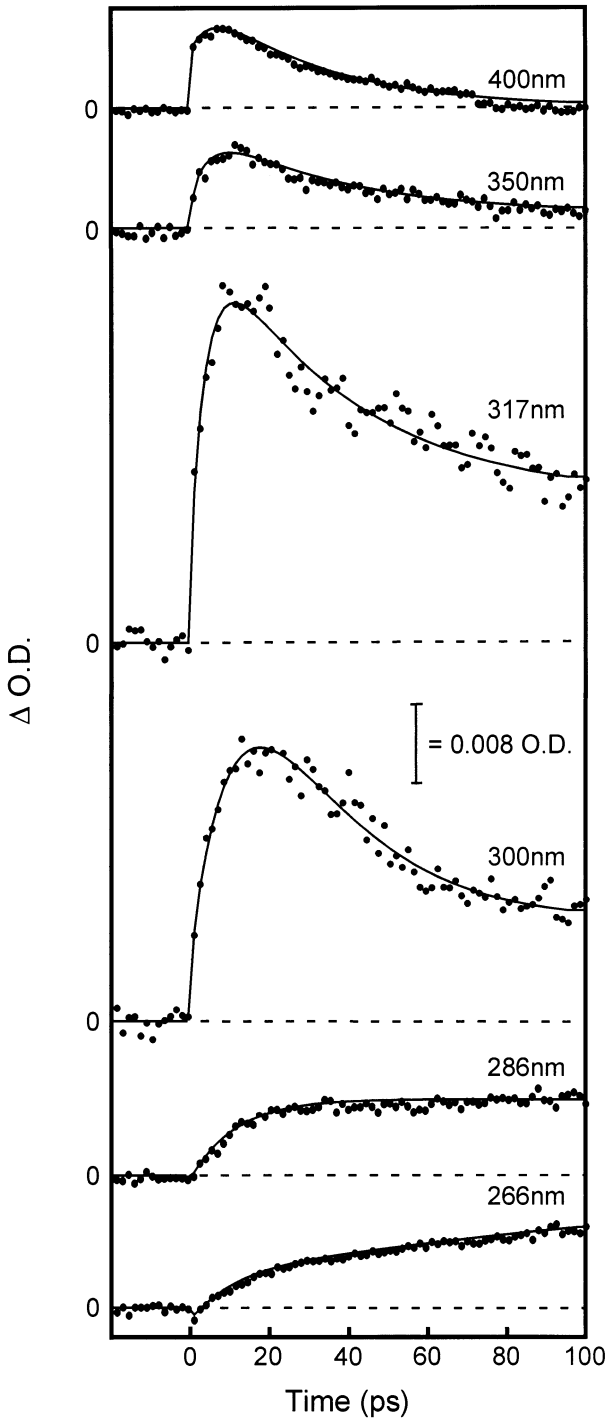

Figure 3. Time-resolved pump−probe dynamics for ClOCl dissolved in perfluorohexane. Probe wavelengths and optical density scale are given in the figure. Best fit to the data by a sum of exponentials convolved with the instrument response is given by the solid line, with corresponding fit parameters presented in Table 1.

time constant of 9.3 ± 4.3 ps and decays with time constants of 26.4 ± 6.2 and 199.3 ± 118.3 ps. As will be discussed below, the amplitude of the optical density increase observed in this wavelength region is significantly greater than the corresponding depletion due to ClOCl photolysis. Therefore, these data demonstrate that following ClOCl photolysis, a photoproduct is formed whose absorption cross section is significantly greater than that of the parent compound.

350 nm ≤ λ_{pr}. In this wavelength region, an increase in optical density is observed that is modest in amplitude relative to the 300 and 317 nm data. At 350 nm, this optical density increase occurs with a time constant of 3.2 ± 1.3 ps and undergoes subsequent biphasic decay with time constants of 28.3 ± 12.6 and 196.2 ± 56.9 ps. Similar behavior is observed at 400 nm, where an instrument-response-limited increase in optical density is observed, which undergoes a subsequent increase with a time constant of 7.9 ± 3.4 ps. The optical density evolution at 400 nm ends by single-exponential decay with a time constant of 20.1 ± 6.7 ps.

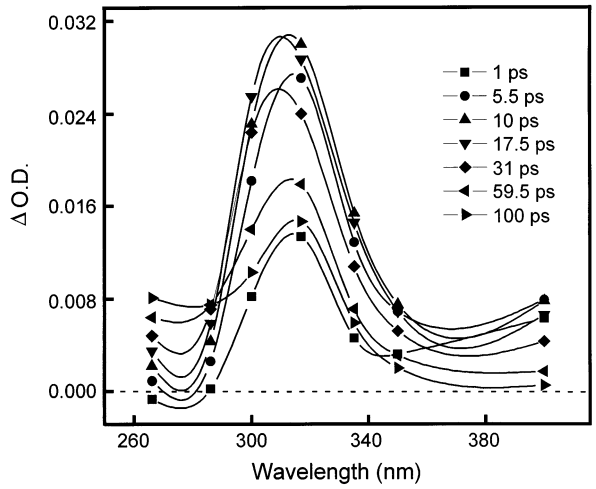

Figure 4. The transient absorption spectra of ClOCl dissolved in perfluorohexane. The time delay for each spectrum is labeled in the figure.

Transient Absorption Spectra. In addition to the single-wavelength studies presented above, the temporal evolution of the absolute optical density change as a function of probe wavelength was determined as presented in Figure 4. There are two major features evident in these data, the depletion and subsequent increase in optical density at 266 nm and the increase and subsequent decay in optical density at ∼315 nm. Following photolysis, depletion at 266 nm is evident consistent with ClOCl ground-state depletion due to photolysis. Studies of the optical density change at early times employing finer time resolution (data not shown) established a maximum optical-density depletion of 0.008 ± 0.002 due to photolysis of ClOCl. In addition to this depletion, an increase in optical density centered at ∼315 nm appears. As the depletion at 266 nm begins to grow steadily into an absorption, the absorption at 315 nm also increases, reaching a maximum of 0.030 OD at 17.5 ps. This absorption then decreases to 0.014 OD by 100 ps. Comparison of the maximum optical density for this feature to the 0.008 OD depletion of ClOCl suggests that the species giving rise to the strong absorption evident in Figure 4 has an extinction coefficient that is 3.75 times greater than the ∼600 M^{-1} cm^{-1} value for ClOCl at 266 nm. This simple analysis assumes that all photoexcited ClOCl results in the production of the 315-nm absorbing photoproduct, an assumption that will revisited below.

In summary, the results presented in Figure 4 demonstrate that ClOCl photolysis results in the production of two species that absorb at 315 and 266 nm. In addition to this result, there are two other features evident in Figure 4 that should be noted. There is a small optical density change at 400 nm observed following photolysis, which quickly reaches a maximum of 0.008 OD before undergoing complete decay. This behavior is consistent with the expected red-edge enhancement of the absorption cross section accompanying vibrational excitation for the species responsible for the 315-nm absorption band.

Finally, there is an apparent isosbestic point at 286 nm for times greater than 17.5 ps. The observation of an isosbestic point suggests that the evolution in optical density in this wavelength region is well modeled as a two-component system, with decay of the species responsible for the 315 nm absorption band resulting in the production of the species absorbing at 266 nm.

Discussion

Discussion of the results presented above is predicted on assignment of the optical-density evolution to those products formed following ClOCl photolysis. As discussed in the Introduction, the potential photolysis products and their corresponding molar absorptivities are presented in Figure 1. The species presented in the figure represent those photoproducts observed in previous studies of ClOCl photochemistry in all phases. Inspection of Figure 1 reveals that the current information regarding photoproduct absorption cross sections cannot be used to make a straightforward assignment of the evolution at 315 nm. However, the simple estimate molar extinction coefficient for the 315-nm absorbing species derived above (2300 M^{-1} cm^{-1}) is most consistent with the production of ClClO, which has a molar extinction coefficient of 3400 M^{-1} cm^{-1} when isolated in low-temperature matrixes.[46] Previous studies of ClClO production following ClOCl photolysis were performed in argon matrixes where the formation of ClClO was evident by the appearance of an absorption band centered at 260 nm. Therefore, assignment of the 315-nm absorption band observed in this study to ClClO requires that the absorption-band maximum of this species undergoes a 55-nm shift between a low-temperature argon matrix and perfluorohexane. We will revisit this issue below after discussing other possible assignments.

A second possible assignment for the 315-nm absorbing species is that it corresponds to ClO. However, in both the gas phase and water, absorption of this species has a maximum of 280 nm (Figure 1). In addition, the molar absorptivity of this compound is only slightly larger than that of ClOCl such that assignment of the 315-nm absorption band to ClO is questionable. Some ClOCl photolysis studies have observed the formation of ClOOCl;[22,45] however, it is doubtful that this species is responsible for the absorption intensity at 315 nm. In addition to the modest molar absorptivity of this compound (Figure 1), this photoproduct is formed by a bimolecular process that should be reflected by concentration dependence of the observed kinetics. The evolution in optical density did not change with a 2-fold change in concentration suggesting that bimolecular processes are not responsible for the observed photoproduct formation dynamics (data not shown).

The final photoproducts to consider are molecular and atomic chlorine. Molecular chlorine does have an absorption maximum at 330 nm, but the extinction coefficient for this transition is only 66 M^{-1} cm^{-1}, far below the estimate for the molar absorptivity of the 315-nm absorbing species presented above.[51] Studies of gaseous ClOCl have observed atomic chlorine production; however, the absorption bands of atomic chlorine are located in the far-UV, removed from the wavelength region of interest. That said, it is possible that atomic chlorine forms a charge-transfer complex with the solvent; however, the high ionization potential of perfluorohexane (16.6 eV) should result in a charge-transfer absorption band maximum of ~162 nm.[52] Therefore, it is doubtful that molecular or atomic chlorine are responsible for the substantial changes in absorption intensity observed at 315 nm.

Given the above, we propose the following assignments for the pump−probe results presented here. The 315-nm absorption band is assigned to ClClO since it is the only species with the requisite molar absorptivity to account for the observed magnitude of optical-density evolution. Regarding the necessity of a 55-nm shift in absorption-band position between the argon matrix studies and this work for this assignment to hold, theoretical calculations of the vertical excitation energies for gaseous ClClO predict that the only electronic transition with significant oscillator strength occurs at 298 nm, in agreement with our assignment.[53] Therefore, the question becomes why one would expect any difference between the ClClO absorption band maximum observed in low-temperature matrixes and that predicted by theory. A potential answer to this question is found in the environmental dependence of the ClClO molecular structure. The IR absorption spectra of ClClO isolated in argon and nitrogen matrixes indicate that the two chlorine atoms are not equivalent and that the frequency of the Cl−O stretch is only slightly shifted from that of isolated ClO.[22] These observations indicate that in the matrix, ClClO is structurally perturbed with an exceedingly weak Cl−Cl bond. Sensitivity of the Cl−Cl bond strength to environment will be reflected by environmental dependence of the ClClO potential energy surfaces. The Cl−Cl bond is expected to be weaker in matrixes relative to the gas phase due to the polarizability of the surrounding matrix. Although one would generally expect similar behavior in solution, the polarizability of perfluorohexane is quite modest. As such, the Cl−Cl bond should be stronger, and the structure of ClClO will correspondingly be more proximate to that of gaseous ClClO. Therefore, a shift of the ClClO absorption-band maximum between low-temperature matrixes and perfluorohexane is not unreasonable.

The increase in optical density observed at 266 nm (Figures 3 and 4) is assigned to production of ClO. Comparison to the 315-nm absorption band suggests that the absorbing species at 266 nm has a smaller molar absorptivity; however, comparison to the reduction in optical density at 266 nm corresponding to ClOCl depletion demonstrates that the molar absorptivity of this species is greater than that of ClOCl. Given the discussion presented above and the data presented in Figure 1, ClO is the only reasonable assignment for optical-density evolution at 266 nm.

Further support for these assignments is found in the resonance Raman studies of Esposito et al.[49] In this work, resonance Raman spectra of ClOCl in CCl_4 were obtained with excitation at 282.4 nm as a function of pulse energy. Figure 5 presents the power dependence of the ClOCl resonance Raman spectrum. The spectra represents the scattering intensities integrated over the temporal duration of the laser pulse (~5 ns) such that all species formed to an appreciable extent, and that have a significant scattering cross sections at this excitation wavelength, will be observed. Figure 5A is the spectrum obtained with a pulse energy of 57 μJ providing for significant photolysis. Figure 5B is the spectrum obtained with a pulse energy of 6.7 μJ corresponding to limited photolysis. By subtraction of the low-energy spectrum from that obtained at high pulse energy, scattering assignable to the photoproducts is observed (Figure 5C). In this difference spectrum, scattering assignable to ClClO and ClO is evident, demonstrating that these two species are produced following ClOCl photoexcitation and that these species have appreciable Raman scattering cross sections consistent with the presence of oscillator strength in this wavelength region.

The proposed ClOCl photochemical reaction dynamics that occur following photoexcitation at 266 nm is presented in Figure 6. Photoexcitation of ground-state ClOCl results in photoi-

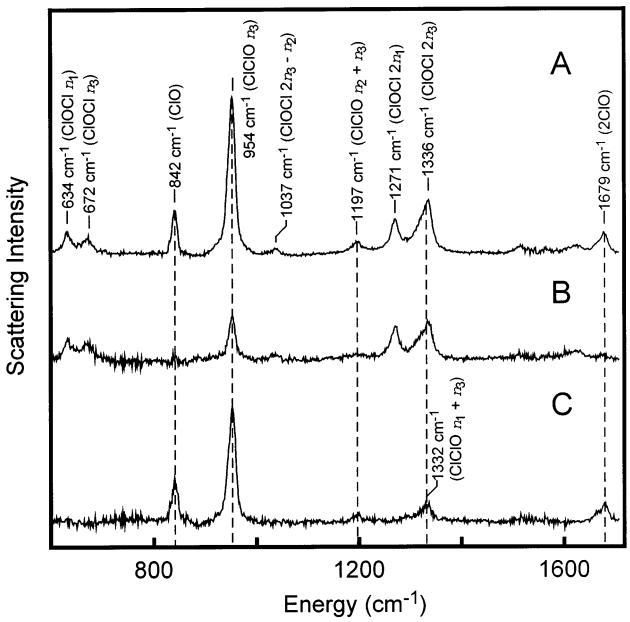

Figure 5. (A) Resonance Raman spectrum of ClOCl in CCl_4 obtained with 57 μJ/pulse at 282.4 nm. Scattering due to ClOCl, ClClO, and ClO is observed. (B) Resonance Raman spectrum of ClOCl in CCl_4 obtained with 6.7 μJ/pulse at 282.4 nm. Scattering due to ClOCl is still present, but scattering due to ClClO and ClO has diminished with the decrease in pulse energy. (C) Difference spectrum generated by subtracting (B) from (A) until the scattering due to ClOCl has vanished. This demonstrates that the only photoproducts of ClOCl are ClClO and ClO.

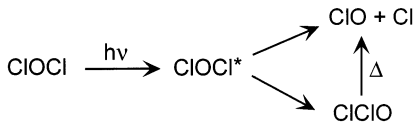

Figure 6. Proposed reaction scheme for the photolysis of ClOCl in perfluorohexane. Excitation of ClOCl results in photodissociation to produce ClO and Cl and photoisomerization to produce ClClO. Following the initial photoproduct production, thermal dissociation of ground-state ClClO results in the production of ClO and Cl.

somerization of the parent molecule to form ClClO as evidenced by the appearance of a strong absorption at 315 nm. In addition, primary dissociation to form ClO and Cl occurs as evidenced by an increase in optical density at 266 nm. Both photoproducts appear on the ~10-ps time scale. Following these dynamics, the isosbestic point at 286 nm for times greater than 17.5 ps is consistent with the thermal decomposition of ClClO resulting in ClO and Cl production on the ~100-ps time scale. The description of the reaction dynamics presented in Figure 6 is basic, with effects such as vibrational relaxation not included in the description at present. It is possible that the photoproduct appearance times represent a combination of photoproduct production and subsequent vibrational relaxation. However, overlap of the photoproduct absorption bands (Figure 1) makes the deconvolution of these effects based on the transient absorption data rather ambiguous. Experiments better suited to such a deconvolution are currently underway.

Given the model presented above, analysis of optical density evolution evident in Figure 4 allows us estimate the quantum yields for ClO and ClClO production. As noted above, an isosbestic point is observed for delay times greater than 17.5 ps consistent with the evolution of a two-component system assigned to the thermal decomposition of ClClO to produce ClO. Given this observation, we define the quantum yield for photoproduct production as that determined by their respective concentrations at 17.5 ps and write

$$1 = \phi_{\mathrm{ClClO}}(17.5\ \mathrm{ps}) + \phi_{\mathrm{ClO}}(17.5\ \mathrm{ps})$$

The 0.008 reduction in optical density at 266 nm (see above) resulting from ground-state ClOCl depletion corresponds to a concentration of 6.5×10^{-5} M. The total optical density change of 0.003 OD observed at 17.5 ps at 266 nm contains a -0.008 ± 0.002 OD contribution from ClOCl depletion; therefore, the optical density originating from ClO is 0.011 ± 0.002 OD (assuming only ClO and ClOCl contribute to the optical density at 266 nm). Using this optical density and the 0.2-cm cell path length employed, we can determine the concentration of ClO by simply using the literature value for the molar extinction coefficient of this species. Two choices for this constant are available: ~800 M^{-1} cm^{-1} for aqueous ClO,[54] and 1386 M^{-1} cm^{-1} for gaseous ClO.[51] Considering that the solvent employed here is devoid of significant intermolecular interactions (see above), we have employed the gas-phase extinction coefficient for this analysis. Given this, we calculate a ClO concentration at 17.5 ps of $(4.0 \pm 0.7) \times 10^{-5}$ M such that the quantum yield for ClO production is 0.6 ± 0.1, and the corresponding quantum yield for ClClO production is 0.4 ± 0.1. By use of this quantum yield for ClClO production and the 0.030 OD observed at 17.5 ps, the molar extinction coefficient for this species at 315 nm is estimated to be 5700 ± 1100 M^{-1} cm^{-1}, which is the expected magnitude for this species.

With respect to halooxide reactivity as a whole, the ClOCl photochemical model presented here has many similarities with the solution-phase behavior observed for OClO. As mentioned above, geminate recombination and photoisomerization play prominent roles in the photochemical reaction dynamics of OClO in solution.[6] The model for ClOCl presented here does not include geminate recombination for the following reason. In the case of aqueous OClO, ~90% of the photoexcited OClO molecules undergo dissociation in to ClO and O which subsequently recombine with a quantum yield of 0.9 ± 0.1.[30,31] However, in a weakly associating solvent such as fluorotrichloromethane, only 30% of the ClO and O photofragments undergo geminate recombination.[35] Given that the studies described here are performed in perfluorohexane, it is likely that the extent of geminate recombination is modest. On comparison of ClOCl and OClO, photoisomerization occurs for both species, with appearance and decay of the isomers (ClClO and ClOO, respectively) occurring on similar time scales.[35] Therefore, it appears that photoisomerization is a general feature of halooxide photochemistry in solution. However, the optical-density assignments discussed above need to be verified in order to confirm the proposed model and quantum yields provided here.

Conclusion

We have presented the first femtosecond transient absorption studies of ClOCl photochemistry in solution. Photolysis of ClOCl at 266 nm in perfluorohexane results in both ClClO and ClO production, with these species appearing on the ~10-ps time scale. Following ClClO production, ground-state thermal decomposition of this species occurs on the ~100-ps time scale resulting in the production of ClO and Cl. If one compares the solution-phase photochemistry of ClOCl to that of OClO, photolysis of both halooxides results in the production of their respective structural isomers. Furthermore, the production and decay kinetics of these isomers occurs on similar time scales suggesting that photoisomerization is a general feature of halooxide photochemistry in solution.

Acknowledgment. The authors thank Matthew Sulham and Gordon Mitchell for their assistance in the preparation of ClOCl. The National Science Foundation is acknowledged for their support of this work (CHE-0091320). Acknowledgment is also made to the donors of the Petroleum Research Fund, administered by the American Chemical Society (P.J.R.). P.J.P. is an Alfred P. Sloan Fellow and is a Cottrell Scholar of the Research Corporation. C.C.C. would like to thank the Ford Foundation for support through an environmental sciences fellowship.

References and Notes

(1) Rowland, F. S. *Annu. Rev. Phys. Chem.* **1991**, *42*, 731.
(2) Renard, J. B.; Pirre, M.; Robert, C.; Huguenin, D. *J. Geophys. Res.* **1998**, *103*, 25383.
(3) Solomon, S.; Borrmann, S.; Garcia, R. R.; Portmann, R.; Thomason, L.; Poole, L. R.; Winker, D.; McCormick, M. P. *J. Geophys. Res.* **1997**, *102*, 21411.
(4) Donsig, H. A.; Herridge, D.; Vickerman, J. C. *J. Phys. Chem. A* **1998**, *102*, 2302.
(5) Vaida, V.; Simon, J. D. *Science* **1995**, *268*, 1443.
(6) Reid, P. J. *J. Phys. Chem. A* **2002**, *106*, 1473.
(7) Molina, M. J.; Tso, T.-L.; Molina, L. T.; Wang, F. C.-Y. *Science* **1987**, *238*, 1253.
(8) Renard, J. J.; Bolker, H. I. *Chem. Rev.* **1976**, *76*, 487.
(9) Davis, H. F.; Lee, Y. T. *J. Phys. Chem.* **1992**, *96*, 5681.
(10) Davis, H. F.; Lee, Y. T. *J. Phys. Chem.* **1996**, *100*, 8142.
(11) Bishenden, E.; Haddock, J.; Donaldson, D. J. *J. Phys. Chem.* **1991**, *95*, 2113.
(12) Bishenden, E.; Donaldson, D. J. *J. Chem. Phys.* **1993**, *99*, 3129.
(13) Bishenden, E.; Donaldson, D. J. *J. Chem. Phys.* **1994**, *101*, 9565.
(14) Baumert, T.; Herek, J. L.; Zewail, A. H. *J. Chem. Phys.* **1993**, *99*, 4430.
(15) Delmdahl, R. F.; Bakker, B. L. G.; Parker, D. H. *J. Chem. Phys.* **2000**, *112*, 5298.
(16) Delmdahl, R. F.; Ullrich, S.; Gericke, K. H. *J. Phys. Chem. A* **1998**, *102*, 7680.
(17) Delmdahl, R. F.; Baumgartel, S.; Gericke, K.-H. *J. Chem. Phys.* **1996**, *194*, 2883.
(18) Roth, M.; Maul, C.; Gericke, K. H. *J. Chem. Phys.* **1997**, *107*, 10582.
(19) Ruhl, E.; Jefferson, A.; Vaida, V. *J. Phys. Chem.* **1990**, *94*, 2990.
(20) Furlan, A.; Scheld, H. A.; Huber, J. R. *J. Chem. Phys.* **1997**, *106*, 6538.
(21) Arkell, A.; Schwager, I. *J. Am. Chem. Soc.* **1967**, *89*, 5999.
(22) Rochkind, M. M.; Pimentel, G. C. *J. Chem. Phys.* **1967**, *42*, 1361.
(23) Peterson, K. A.; Werner, H.-J. *J. Chem. Phys.* **1992**, *96*, 8948.
(24) Mueller, H. S. P.; Willner, H. *J. Phys. Chem.* **1993**, *97*, 10589.
(25) Thøgersen, J.; Jepsen, P. U.; Thomsen, C. L.; Poulsen, J. A.; Byberg, J. R.; Keiding, S. R. *J. Phys. Chem. A* **1997**, *101*, 3317.
(26) Philpott, M. J.; Charalambous, S.; Reid, P. J. *Chem. Phys. Lett.* **1997**, *281*, 1.
(27) Poulsen, J. A.; Thomsen, C. L.; Keiding, S. R.; Thøgersen, J. *J. Chem. Phys.* **1998**, *108*, 8461.
(28) Thøgersen, J.; Thomsen, C. L.; J. Aa. Poulsen; Keiding, S. R. *J. Phys. Chem. A* **1998**, *102*, 4186.
(29) Philpott, M. J.; Charalambous, S.; Reid, P. J. *Chem. Phys.* **1998**, *236*, 207.
(30) Hayes, S. C.; Philpott, M. J.; Reid, P. J. *J. Chem. Phys.* **1998**, *109*, 2596.
(31) Hayes, S. C.; Philpott, M. P.; Mayer, S. G.; Reid, P. J. *J. Phys. Chem. A* **1999**, *103*, 5534.
(32) Thomsen, C. L.; Philpott, M. P.; Hayes, S. C.; Reid, P. J. *J. Chem. Phys.* **2000**, *112*, 505.
(33) Thomsen, C. L.; Reid, P. J.; Keiding, S. R. *J. Am. Chem. Soc.* **2000**, *122*, 12795.
(34) Philpott, M. J.; Hayes, S. C.; Thomsen, C. L.; Reid, P. J. *Chem. Phys.* **2001**, *263*, 389.
(35) Hayes, S. C.; Thomsen, C. L.; Reid, P. J. *J. Chem. Phys.* **2001**, *115*, 11228.
(36) Edgecombe, F. H. C.; Norrish, R. G. W.; Thrush, B. A. *Proc. R. Soc. London* **1957**, *A243*, 455.
(37) Basco, N.; Dogra, S. K. *Proc. R. Soc. London* **1971**, *323*, 401.
(38) Sander, S. P.; Friedl, R. R. *J. Phys. Chem.* **1989**, *93*, 4764.
(39) Chichinin, A. I. *Chem. Phys. Lett.* **1993**, *209*, 459.
(40) Nelson, C. M.; Moore, T. A.; Okumura, M.; Minton, T. K. *J. Chem. Phys.* **1994**, *100*, 8055. Moore, T. A.; Okumura, M.; Minton, T. K. *J. Chem. Phys.* **1997**, *107*, 3337.
(41) Nickolaisen, S. L.; Miller, C. E.; Sander, S. P.; Hand, M. R.; Williams, I. H.; Francisco, J. S. *J. Chem. Phys.* **1996**, *104*, 2857.
(42) Aures, R.; Gericke, K.-H.; Maul, C.; Trott-Kreigeskorte, G. *J. Chem. Phys*. **2002**, *117*, 2141.
(43) Tanaka, Y.; Kawasaki, M.; Matsumi, Y.; Fujiwara, H.; Ishiwata, T.; Rogers, L. J.; Dixon, R. N.; Ashfold, M. N. R. *J. Chem. Phys.* **1998**, *109*, 1315.
(44) Smith, G. D.; Tablas, F. M. G.; Molina, L. T.; Molina, M. J.*J. Phys. Chem. A* **2001**, *105*, 8658.
(45) Chi, F. K.; Andrews, L. *J. Phys. Chem.* **1973**, *77*, 3062.
(46) Johnsson, K.; Engdahl, A.; Nelander, B. *J. Phys. Chem.* **1995**, *99*, 3965.
(47) Gane, M. P.; Williams, N. A.; Sodeau, J. R. *J. Chem. Soc., Faraday Trans.* **1997**, *93*, 2747.
(48) Dickinson, R. G.; Jeffreys, C. E. P. *J. Am. Chem. Soc.* **1930**, *52*, 4288.
(49) Esposito, A. P.; Reid, P. J.; Rousslang, K. W. *J. Photochem. Photobiol. A* **1999**, *129*, 9.
(50) Cady, G. H. *Inorg. Synth.* **1957**, *5*, 156.
(51) Demore, W. B.; Sander, S. P.; Golden, D. M.; Hampson, R. F.; Kurylo, M. J.; Howard, C. J.; Ravishankara, A. R.; Kolb, C. E.; Molina, M. J. In *Chemical Kinetics and Photochemical Data for Use in Stratospheric Modeling*; NASA Contractor Report CR-198863; NASA Jet Propulson Laboratory, California Institute ofTechnology, Pasadena, CA, 1994.
(52) Chateauneuf, J. E. *Chem. Phys. Lett.* **1989**, *164*, 577.
(53) Delbene, J. E.; Watts, J. D.; Bartlett, R. J. *Chem. Phys. Lett.* **1995**, *246*, 541.
(54) Klaning, U. K.; Wolff, T. *Ber. Bunsen-Ges. Phys. Chem.* **1985**, *89*, 243.
(55) Anbar, M.; Dostrovsky, I. *J. Chem. Soc.* **1954**, 1105.